



The study of electrochemical properties and lithium deposition of graphite at low temperature

Gumjae Park^a, Nanda Gunawardhana^a, Hiroyoshi Nakamura^a, Yun-Sung Lee^b, Masaki Yoshio^{a,*}

^a Department of Applied Chemistry, Saga University, 1 Honjo, Saga 840-8502, Japan

^b Faculty of Applied Chemical Engineering, Chonnam National University, 300 Yongbong-dong, Gwangju 500-757, Republic of Korea

ARTICLE INFO

Article history:

Received 29 June 2011

Received in revised form 29 August 2011

Accepted 17 October 2011

Available online 20 October 2011

Keywords:

Graphite

Graphitization

Rhombohedral phase

Li intercalation

Li deposition

ABSTRACT

The electrochemical properties of graphite with various degrees of graphitization, contents of rhombohedral phase, and surface areas were electrochemically investigated at 25 °C and −5 °C. The degree of graphitization and the amount of rhombohedral phase affected the samples' lithium intercalation/deintercalation and surface deposition. The reductions of electrolyte conductivity and lithium ion diffusion in the graphite interlayer at −5 °C lowered the graphite's capacity. Lithium deposition also occurred on the graphite's surface. Highly graphitized samples were affected greatly by temperature, showing large capacity loss at low temperature. Increased rhombohedral phase facilitated lithium deposition on the graphite's surface as lithium ions did not insert into the graphite interlayers and accumulated at its edged planes. Increasing the pathways for lithium ion intercalation could facilitate lithium intercalation and reduce lithium deposition.

© 2011 Elsevier B.V. All rights reserved.

1. Introduction

Lithium ion batteries (LIBs) are used as power sources for portable devices such as cellular phones, laptop computers, and digital cameras. They are also used in stationary systems, battery-assisted bicycles, and hybrid electric vehicles due to their high energy densities. Graphite commonly forms the anodes of lithium ion batteries because of its low cost and non-toxicity [1]. It has high reversible specific charge (up to 372 mAh g^{−1}), good cycling stability, and high electronic conductivity. Lithium intercalation into graphite occurs at very low potentials (below 0.3 V vs. Li/Li⁺), resulting in high-energy density anodes for LIBs [2].

Although it has numerous advantages, these properties are limited to room temperature and rapidly deteriorated at below 0 °C [3–11]. The research related to these properties at low temperature has been widely carried out. Many researchers have focused on the low ionic conductivity of electrolyte and solid electrolyte interface on the graphite surface in order to develop an electrolyte with low freezing point and high ionic conductivity [3–7]. Indeed, these approaches led to an improved low temperature performance of graphite. Moreover, the recent work have revealed that the electrochemical properties of graphite can be affected by diffusivity of lithium ions into the graphite layers as well as ionic conductivity of the electrolyte when operating at low temperatures

in the lithium ion batteries [8–11]. There are many factors contribute to poor electrochemical performance of graphite at low temperatures. The main reasons are (1) reduced conductivity of the electrolyte and (2) the formation of improper solid electrolyte interface on the electrode surface. It limits slow diffusivity of lithium ions within graphite anode, high polarization of the graphite anode, and substantially increased charge-transfer resistance on the electrolyte–electrode interfaces.

In addition to the poor performance at low temperatures, it is well known that the deposition of lithium metal at the surface of graphite which is likely to form lithium dendrite at low temperatures and high cycling rates [12–14]. Once lithium deposited on the graphite, it grows and reaches the positive electrode as cycle progresses, causing a short circuit in LIBs. It caused the severe safety problems for LIBs and can limit the extension it to large scale battery systems.

It is believed that the morphology and structure have a great effect not only on their electrochemical properties but also lithium deposition on the surface of graphite at low temperatures. In this study, the electrochemical properties of five types of graphite including one natural and four synthetic graphite samples were investigated by the galvanostatic charge/discharge test at low temperature. The lithium deposition on the surface of graphite was also investigated by comparing the colors of electrode and *ex situ* X-ray diffraction analysis after the first charge process. From the result, it was found that the electrochemical properties and lithium deposition at low temperatures strongly related to the surface and original properties of the graphite samples.

* Corresponding author. Tel.: +81 952 28 8591.

E-mail address: yoshio@cc.saga-u.ac.jp (M. Yoshio).

Table 1
Graphite samples' physical properties.

	NG	KS-6	MCMB6-28	MCF	MAGC
Surface area ($\text{m}^2 \text{g}^{-1}$)	0.6	15	2.6	1.2	4.0
d_{002} (nm)	0.3354	0.3365	0.3363	0.3602	0.3359
Graphitization (%)	99.0	86.4	89.0	91.9	93.4
Tentatively 3R (%)	30.9	26.4	0	0	0
Shape	Flake	Plate-like	Sphere	Fiber	Mass
Company	China	Timcal	Osaka gas	Petoca	Hitachi Kasei

2. Experimental

Five representative graphite samples were selected as the negative electrode materials in this study, including natural graphite and synthetic graphite samples: KS-6 (Timcal Co. Ltd), MAGC (Massive Artificial Graphite, Hitachi Kasei), MCMB6-28 (Meso Carbon Microbead, Osaka gas), and MCF (Meso Carbon Fibers, Petoca). Some of their physical properties are listed and compared in Table 1. Powder X-ray diffraction (XRD, MINIFlex II, Rigaku, Japan) using $\text{CuK}\alpha$ radiation was employed to identify the physical properties of graphite sample. In the XRD experiment, we used Si powder as standard material in order to correct the peak of graphite. The morphology of used graphite samples was observed by Scanning Electron Microscopy (SEM, JSM-6390, JEOL, Japan).

All electrochemical cells were fabricated in the dry-box. The charge–discharge tests were performed using a CR2032 coin-type cell. Graphite electrodes were coated on copper foil by doctor blade with a mixture of 90% graphite sample – 6% acetylene black – 4% carboxymethylcellulose (CMC) dispersed in distilled water, dried at 100°C , pressed at 150.0 kg cm^{-2} , and finally dried in a glass tube oven at 160°C for 4 h. The test cell was made of graphite electrodes and a lithium metal anode (Cyprus Foote Mineral Co.) separated by two glass fiber filters. The electrolyte was a mixture of 1 M LiPF_6 -ethylene carbonate (EC)/diethyl carbonate (DEC) (3:7 by vol., Ube Chemicals, Japan). The charge and discharge current densities was 0.1 mA cm^{-2} with a cut-off voltage from 2500 to 5 mV.

For *ex situ* XRD experiment, the electrodes were prepared with 10 mg of accurately weighed active material and 6 mg of conductive binder TAB (Teflonized Acetylene Black). It was pressed onto Ti mesh as current collect under pressure of 150 kg cm^{-2} and dried at 160°C for 4 h. The test cells were charged at a rate of 0.1 mA cm^{-2} to 5 mV and kept 10 h period at that voltage. After completion of this test, the cells were disassembled and rinsed with dimethylcarbonate (DMC) in an argon-filled glove box. The disassembled electrodes were sealed in a vinyl bag in an argon-filled glove box to prevent any reaction with moisture and/or air.

3. Results and discussion

Natural graphite and four commercial artificial graphite samples were characterized. Their XRD patterns were obtained using a Si powder standard to correct the graphite (002) peaks. Fig. 1 shows that all the XRD patterns were typical graphitic materials with sharp (002) peaks indicating good graphitization. High graphitization was demonstrated by the samples' interlayer spacing, d_{002} . The (002) peaks appeared at $2\theta = 26.46\text{--}26.56^\circ$, corresponding to d_{002} values of 0.3665–0.3554 nm. All the graphite samples were indexed using Franklin's definition [15]. These showed small variations related to their fine structures, such as graphitization. The graphitizations of NG, KS-6, MAGC, MCMB6-28, and MCF were 99.0, 86.4, 93.4, 89.0 and 91.9%, respectively. The samples also showed different extents of rhombohedral phase (3R). The more prevalent hexagonal phase (2H) and the rhombohedral phase differ mainly in their stacking sequences of graphene sheets. Four peaks were observed at X-ray diffraction angles of $40\text{--}50^\circ$. The peaks at *ca.* 42.3° and 44.4° are attributable to (100) and (101) planes

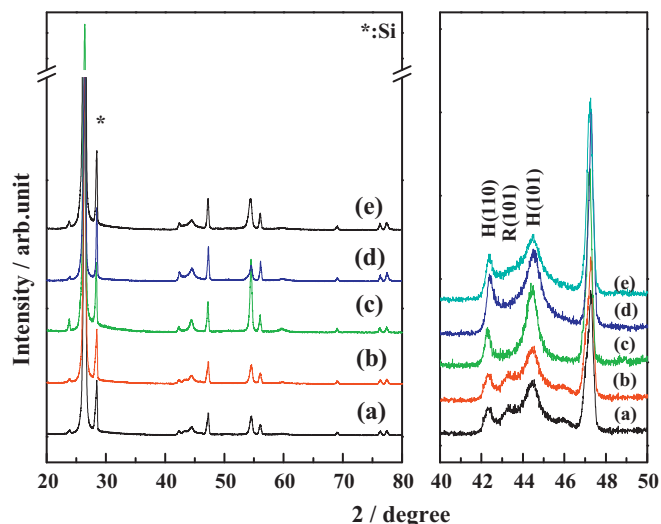


Fig. 1. XRD patterns of graphite samples: (a) NG, (b) KS-6, (c) MAGC, (d) MCMB6-28, and (e) MCF.

of the hexagonal structure, respectively. The (101) and (102) planes of rhombohedral graphite appeared at *ca.* 43.3° and 46.0° , respectively. Accurate estimation was hampered by the peaks being broad, weak, and not particularly separated from the baseline. R3 contents in the NG, KS-6, MAGC, MCMB6-28, and MCF were 30.9, 26.4, 0, 0, and 0%, respectively.

Fig. 2 shows the scanning electron microscopy (SEM) images of used graphite samples in this study. The SEM images show that the natural graphite particles were 10–30 μm flakes and the artificial graphite samples were of various shapes and sizes. The particles of KS-6, MAGC, MCMB6-28, and MCF were 5–10 μm plates, 20–40 μm masses, 10–20 μm spheres, and 5–15 μm fibers, respectively. The KS-6 graphite had a high BET surface area of $15 \text{ m}^2 \text{g}^{-1}$, the other samples all showed values below $4 \text{ m}^2 \text{g}^{-1}$. The properties of all samples are summarized in Table 1.

Fig. 3 shows the first charge/discharge curves of various graphite samples. The first charge/discharge curves were measured at a current density of 0.1 mA cm^{-2} , with voltage cut-off of 2.5–0 V in a 3:7 volume mixture of 1 M LiPF_6 -EC and DEC. Three voltage plateaus at room temperature were observed during charge and discharge in all the samples. They appeared at *ca.* 190, 95, and 65 mV for lithium insertion and at *ca.* 105, 140, and 230 mV for extraction. This was attributed to the transition stages of lithium-graphite intercalation compounds (Li-GICs) formed during lithium insertion or extraction between the graphene layers. These results agreed well with previous report [16]. All the samples showed reversible capacities of over 300 mAh g^{-1} .

On the other hand, at -5°C , the voltage plateaus for lithium intercalation were lower than at room temperature; the lithium extraction plateaus were at higher voltages. The lowest voltage plateaus shown by all samples were unclear due to the formation of LiC_6 at -5°C . The capacities of samples at -5°C were decreased compared with those at room temperature. NG showed

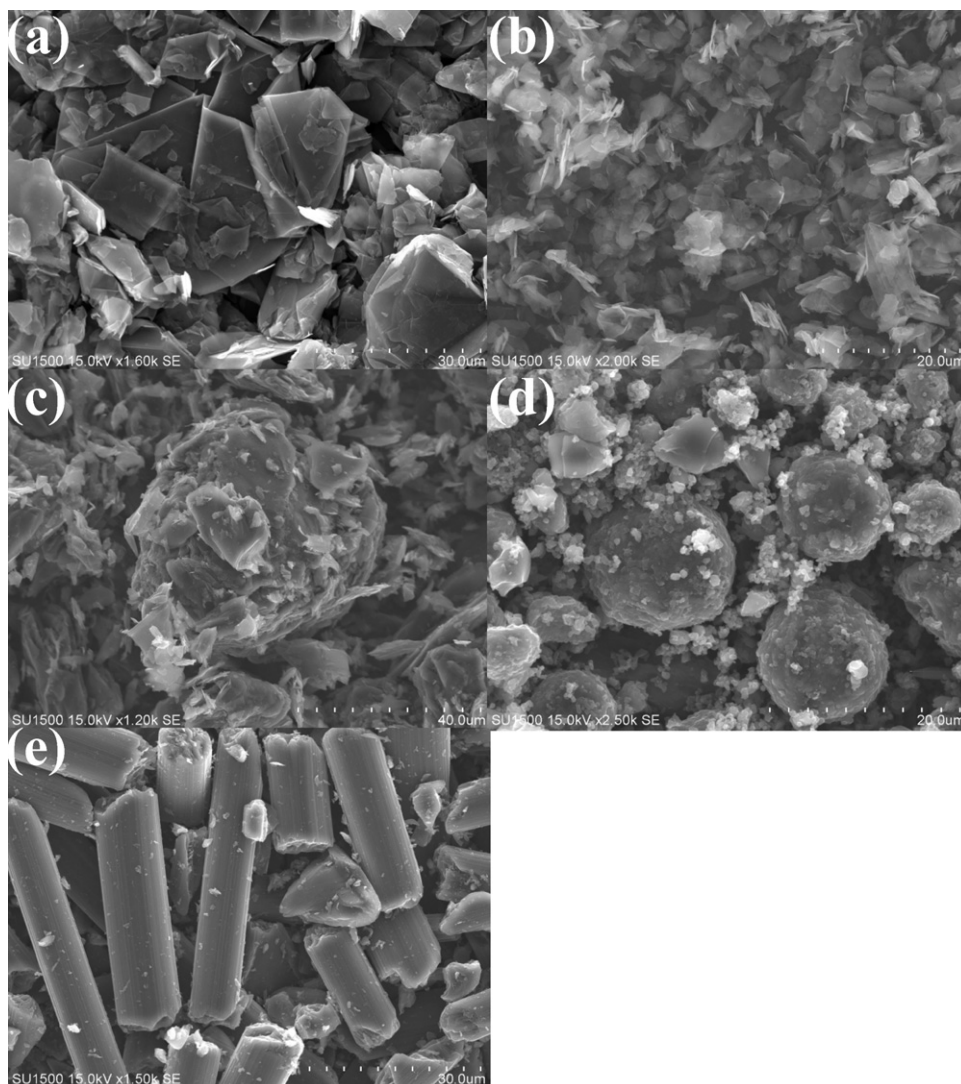


Fig. 2. SEM images of graphite samples: (a) NG, (b) KS-6, (c) MAGC, (d) MCMB6-28, and (e) MCF.

two reversible voltage plateaus at *ca.* 150 and 65 mV for lithium intercalation and at 200 and 250 mV for lithium extraction. KS-6 and MAGC showed three voltage plateaus during charging and discharging, with the capacities at the voltage plateaus for LiC_6 formation being smaller than those at room temperature. MCMB6-28 and MCF showed different charge/discharge curves from the other samples at -5°C . They show rapid decreases to 150 mV, with voltage then slowly decreasing to the end of charging. Voltage increased rapidly to 150 mV and before increasing slowly to 300 mV. The initial discharge capacities of NG, KS-6, MAGC, MCMB6-28, and MCF were 201.7, 301.7, 243.8, 227.1, and 212.1 mAh g^{-1} , respectively. All samples showed large capacity losses from those at 25°C upon cooling to -5°C .

Samples' initial charge/discharge capacities, irreversible capacities, and columbic efficiencies at 25°C and -5°C are listed in Table 2. All samples showed reversible capacities of above 300mAh g^{-1} at 25°C , which dropped to below 250mAh g^{-1} at -5°C , except sample KS-6. The charge/discharge curves show that graphite's electrochemical properties at -5°C were degraded due to the lower conductivity of the electrolyte and hindered lithium diffusion into the graphene layers. Lithium intercalation and graphite's electrochemical properties are affected by the physical properties of the graphite, although quantification of physical

effects on electrochemical properties is difficult [19–30]. The complexity is mainly due to the large variation in graphitization [19,20], particle shape and size [21], impurities, densities of dislocation [22–27], surface area, and surface functional groups of the existing graphite samples [28–30]. These factors are related to the formation of SEI film during the first charge, which suppress graphite's electrochemical exfoliation. Electrochemical exfoliation can be avoided on graphite surfaces with high defect contents, since surface passivation is sufficiently completed at more positive potentials. We believed that the physical properties of graphite have big related to their electrochemical properties at low temperature.

To explore the great effects of its physical properties on its electrochemical properties at low temperature, graphite's physical and low-temperature electrochemical properties were characterized as shown in Fig. 4. Samples' capacity differences upon temperature were explored with respect to their degrees of graphitization. The capacity differences of NG, MAGC, MCF, MCMB6-28, and KS-6 were 148.0, 125.8, 111.9, 100.2, and 38.6 mAh g^{-1} , respectively, with higher graphitization leading to larger capacity losses at low temperature. These results show that the electrochemical properties of graphite at lower temperature (-5°C) depended on its degree of graphitization, with higher graphitization showing greater deterioration of electrochemical properties with temperature changes.

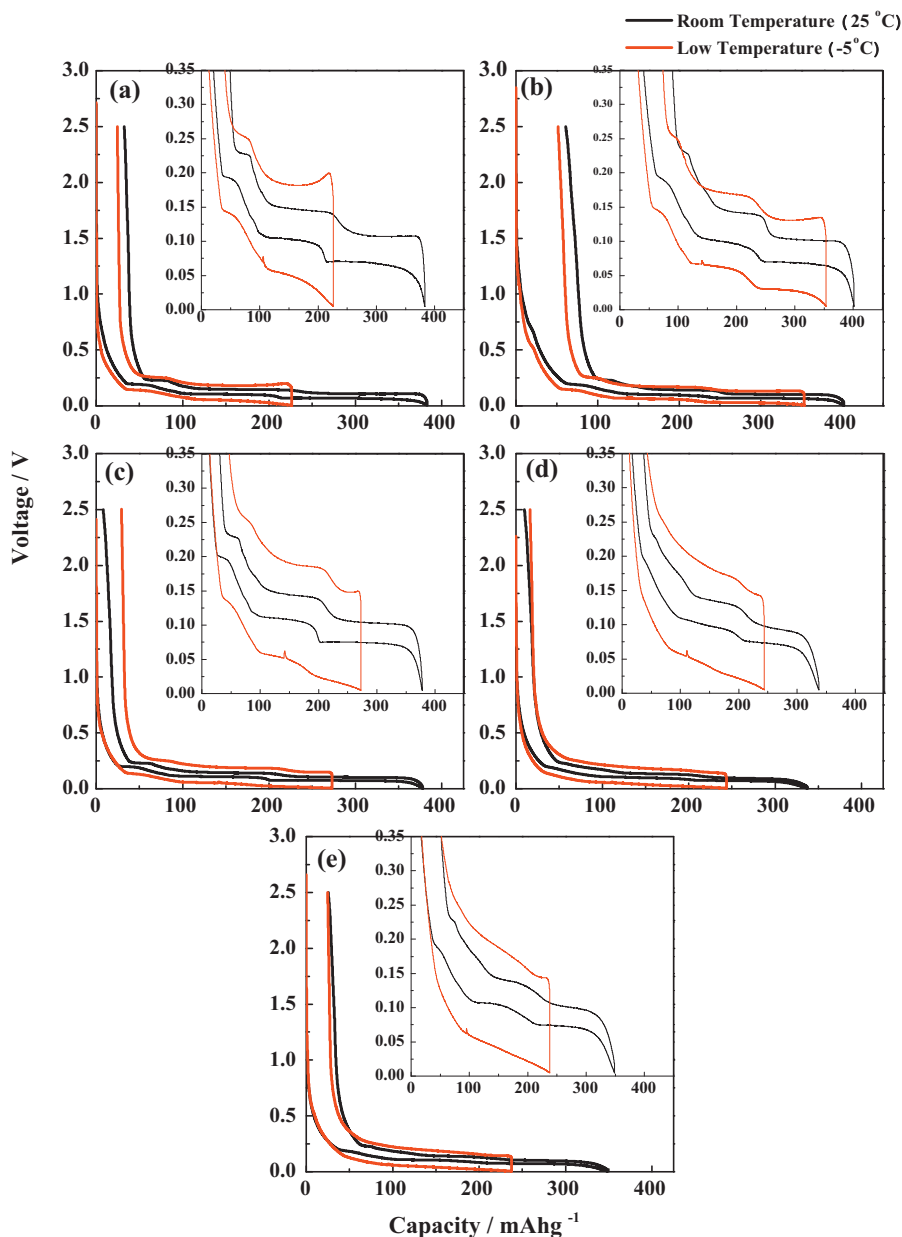


Fig. 3. The first charge–discharge curves of graphite/Li cells in the electrolyte of 1 M LiPF₆-EC/DEC (3:7 by volume): (a) natural graphite, (b) KS-6 graphite, (c) MAGC graphite, (d) MCMB6-28 graphite, and (e) MCF graphite.

Table 2

The first charge/discharge characteristics of the graphite samples.

The type of graphite	Discharge capacity at the first cycle (mAh g ⁻¹)	Charge capacity at the first cycle (mAh g ⁻¹)	Irreversible capacity at the first cycle (mAh g ⁻¹)	Coulombic efficiency at the first cycle (%)
NG				
RT (25 °C)	349.7	382.1	32.4	91.5
LT (-5 °C)	201.7	226.2	24.5	89.2
KS-6				
RT (25 °C)	340.3	401.4	61.0	84.8
LT (-5 °C)	301.7	353.2	51.5	85.4
MAGC				
RT (25 °C)	369.6	377.6	8.0	97.9
LT (-5 °C)	243.8	292.9	29.1	83.2
MCMB6-28				
RT (25 °C)	327.3	337.1	9.8	97.0
LT (-5 °C)	227.1	243.3	16.2	93.3
MCF				
RT (25 °C)	323.0	348.5	25.5	92.6
LT (-5 °C)	212.1	236.7	24.7	89.5

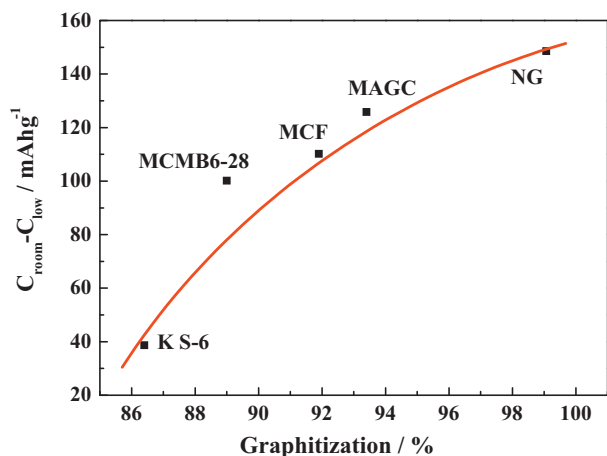


Fig. 4. Low-temperature capacity loss with respect to degree of graphitization.

Lithium deposition on the graphite occurred at -5°C , leading to severe safety problems associated with lithium ion batteries. After first charging, the graphite samples appeared yellow-black as shown in Fig. 5. All colors of graphite samples are consisted with yellow and black. The yellow is attributable to the formation of first-stage lithium-graphite intercalation compounds (GICs) [18]. The black was attributed the second-stage Li GICs and lithium deposition on the graphite's surface. Although there were variations of color, all the samples appeared both yellow and black after first charging, showing that lithium deposition occurred in addition to lithium intercalation during first charging at -5°C .

To confirm this result, it was conducted the *ex situ* XRD after the 1st charge process. Fig. 6 shows *ex situ* XRD results of graphite samples after the 1st charge process. For measurement, the Cu collector was replaced by a titanium collector to avoid

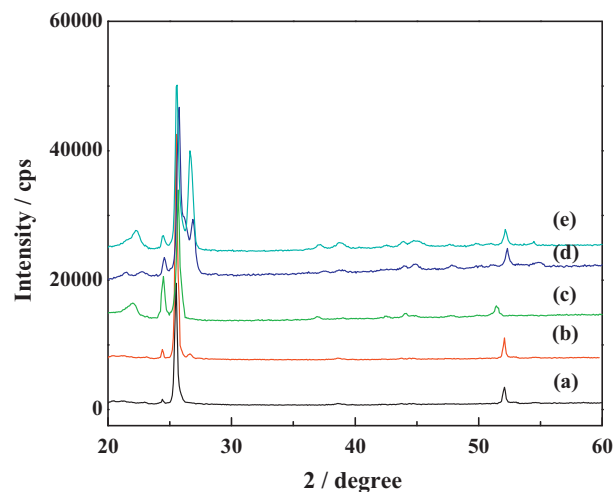


Fig. 6. XRD patterns of graphite samples after the 1st charge with Ti current collector: (a) NG, (b) KS-6, (c) MAGC, (d) MCMB6-28, and (e) MCF.

duplication of Cu ($2\theta = 51^{\circ}$) and Li ($2\theta = 52^{\circ}$) signals from the screw-type cells. Testing was after charging to 5 mV with a current density of 0.1 mA cm^{-2} and holding at 5 mV for 10 h. The original (002) peak of all graphite samples was reduced by charging because of lithium ions intercalated into the graphite layers and the formation of GICs. All samples showed peaks at $2\theta = 24.3^{\circ}$ and $2\theta = 25.4^{\circ}$ corresponding to LiC_6 and LiC_{12} due to the intercalation of lithium [17,31]. This agreed with the result of charge/discharge testing, which showed reduced capacities at the first-stage voltage plateaus at lower temperatures. All samples showed lithium intercalation peaks at $2\theta = 52^{\circ}$. This result suggests that lithium deposition on the surfaces of the graphite samples readily occurred during their first charging.

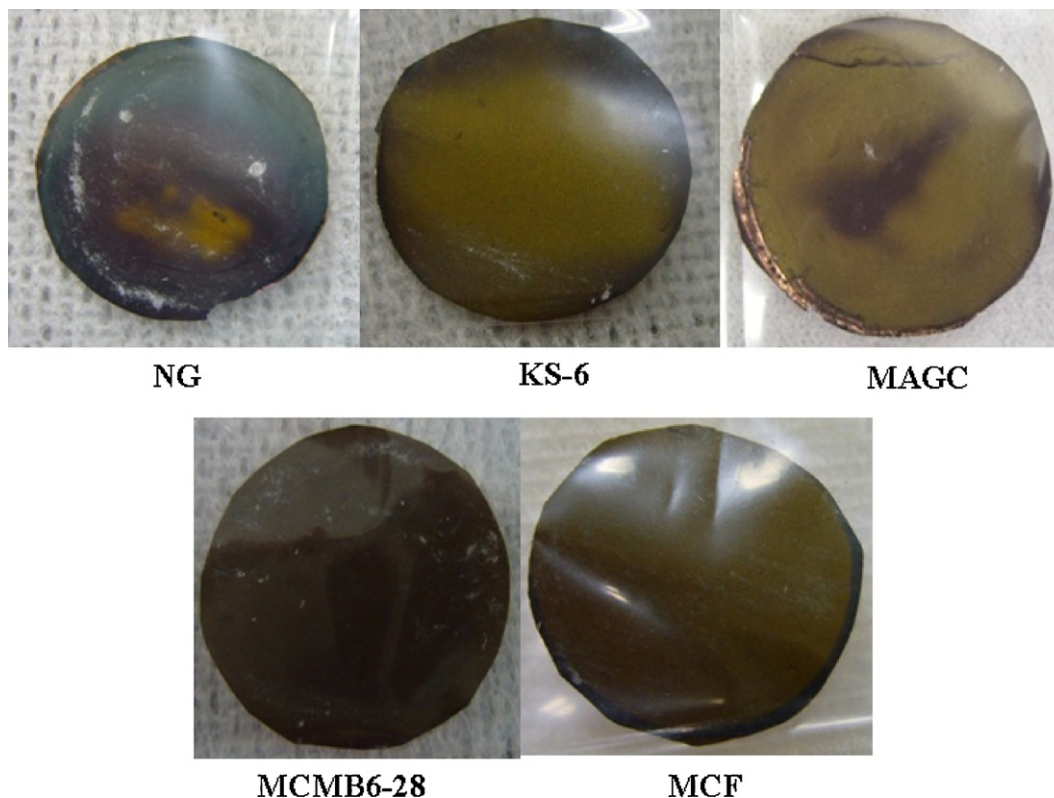


Fig. 5. The appearance of graphite samples after 1st charging: (a) natural graphite, (b) KS-6 graphite, (c) MAGC graphite, (d) MCMB6-28 graphite, and (e) MCF graphite.

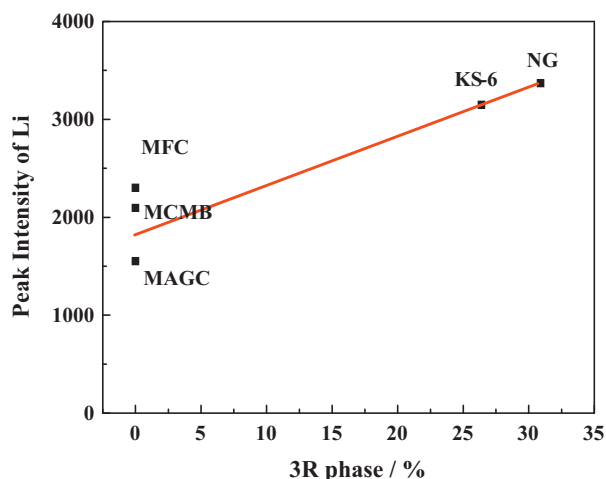


Fig. 7. Li_6 peak intensities with respect graphite's to rhombohedral stacking.

Fig. 7 shows the plot of intensity of LiC_6 dependence on the rhombohedral phase in graphite samples. The relationship between the contents of rhombohedral phase in graphite and the degree of the lithium deposition was investigated at -5°C after the first charge process by *ex situ* XRD. Lower contents of rhombohedral phase resulted in higher intensity lithium peaks. Since the conductivity of the electrolyte and lithium ion diffusion in the graphene layers were reduced at -5°C , the lithium ion could accumulate on the graphite's edged planes and did not insert into its basal planes. There are two general ordering patterns of stacked graphene layers: hexagonal, ABAB, and rhombohedral, ABCABC. Greater rhombohedral stacking results in higher reversible capacities [21–26]. It also provides less vulnerability to solvent co-intercalation because of the higher number of structural defects such as grain boundaries and dislocations, which hinder the movement of large molecules inside the graphite but allow small unsolvated lithium cations to penetrate the bulk graphite. Increased rhombohedral stacking increases lithium storage capacity due to lithium being stored at grain boundaries in the graphite in addition to lithium intercalation between the graphene layers. As reaching the low temperature, however, the conductivity of the electrolyte and lithium ion diffusion in the graphene layers reduced during charging due to lithium deposition on the graphite becoming possible on grain boundaries of the rhombohedral and hexagonal phases.

The samples with no rhombohedral stacking, MAGC, MCMB6-28 and MCF, showed different degrees of lithium deposition. Therefore, in addition to rhombohedral phase content, particle shape also likely affected lithium deposition. After being cast on the current collector and pressed, the particles' *c*-axes aligned in various ways. MCF has a radical-like texture in the outer surface, together with a lamellar structure in the core [32]. Lithium was intercalated through the radical-like texture in the skin part. As MCMB6-28 is spherical type graphite, in which the most of surface are composed of edge-plane, thus lithium ion easily intercalated into basal plane [33]. MAG consists of spherical aggregation of fine, flat crystals [34]. In the core of MAGC, primary flat particles are randomly aggregated with wide range of pore sizes. These new pores become the path to lithium ion intercalation after soaked by electrolyte. Thus, the intercalation and de-intercalation can be carried out not only on the outer surface which resulted in accelerating lithium ion intercalation into graphite. Increased contact area between the graphite's edged planes and the electrolyte facilitated lithium ion intercalation and extraction. High-surface area graphite without rhombohedral phases showed more facile intercalation of lithium into its interlayers, with increased lithium intercalation through the edged planes rather than accumulating on the edged planes.

In the present study, we investigated the factors affecting the electrochemical properties and lithium deposition of graphite electrode at low temperature. The factors such as degree of graphitization and the amount of rhombohedral phase in graphite play crucial role for the lithium intercalation/deintercalation and lithium deposition of graphite samples. Appropriate manipulation of these factors could improve the safety of graphite electrodes for use in hybrid and electric vehicles.

4. Conclusion

The electrochemical performances of various graphite samples were assessed at low temperature. Charge/discharge testing showed that voltage plateaus due to the intercalation of lithium ions into graphene layers were lower at low temperature; those due to lithium extraction were higher. This was due to reduced electrolyte conductivity and decreased lithium diffusion in the graphene. High degrees of graphitization were more greatly affected by the reduction of temperature. All the graphite samples showed lithium deposition on their surfaces at low temperature. Increased rhombohedral graphite stacking facilitated lithium deposition on the graphite's surface because lithium ions could not insert into graphite's interlayers; they accumulated at the edged planes. Graphite particles' shapes and surface areas also affected electrochemical performance. Increasing the pathway for the intercalation of lithium ions into the graphite facilitated lithium intercalation and decreased lithium deposition on the graphite's surface. We believe that an appropriate condition of those factors could improve the safety of graphite to satisfactory for HEV and EV application.

Acknowledgements

This work was partially supported by Energy Resource R&D program under the Ministry of Knowledge Economy, Republic of Korea.

References

- [1] M. Noel, R. Santahnam, J. Power Sources 72 (1998) 53.
- [2] J.R. Dahn, A.K. Sleight, H. Shi, J.N. Reimers, Q. Zhong, B.M. Way, Electrochim. Acta 38 (1993) 1179.
- [3] M.C. Smart, B.V. Ratnakumar, S. Surampudi, J. Electrochem. Soc. 146 (1999) 486.
- [4] H.C. Shiao, D. Chua, H.P. Lin, S. Slane, M. Salomon, J. Power Sources 87 (2000) 167.
- [5] E.J. Plichta, W.K. Behl, J. Power Sources 88 (2000) 192.
- [6] E.J. Plichta, M. Hendrickson, R. Thompson, G. Au, W.K. Behl, M.C. Smart, B.V. Ratnakumar, S. Surampudi, J. Power Sources 94 (2001) 160.
- [7] S. Herreyre, O. Huchet, S. Barusseau, F. Pertion, J.M. Bodet, P. Biensan, J. Power Sources 97–98 (2001) 576.
- [8] C.K. Huang, J.S. Sakamoto, J. Wolfenstine, S. Surampudi, J. Electrochem. Soc. 147 (2000) 486.
- [9] H.P. Lin, D. Chua, M. Salomon, H.C. Shiao, M. Hendrickson, E. Plichta, S. Slane, Electrochem. Solid-State Lett. 4 (2001) A71.
- [10] S.S. Zhang, K. Xu, J.L. Allen, T.R. Jow, J. Power Sources 110 (2002) 217.
- [11] S.S. Zhang, K. Xu, T.R. Jow, Electrochim. Acta 48 (2002) 241.
- [12] H. Honbo, K. Takei, Y. Ishii, T. Nishida, J. Power Sources 189 (2009) 337.
- [13] Y. Reynier, R. Yazami, B. Fultz, J. Power Sources 189 (2009) 602.
- [14] G. Park, H. Nakamura, Y. Lee, M. Yoshio, J. Power Sources 189 (2008) 602.
- [15] R.E. Franklin, Acta Crystallogr. 4 (1951) 235.
- [16] D. Guerard, A. Herold, Carbon 13 (1975) 337.
- [17] J. Ohzuku, Y. Iwakoshi, K. Sawai, J. Electrochem. Soc. 140 (1993) 2490.
- [18] J.R. Dahn, Phys. Rev. B 44 (1991) 9170.
- [19] L.J. Hardwick, H. Buqa, M. Holzapfel, W. Scheifele, F. Krumeich, P. Novak, Electrochim. Acta 52 (2007) 4884.
- [20] C.S. Wang, G.T. Wu, W.Z. Li, J. Power Sources 76 (1998) 1.
- [21] H. Shi, J. Barker, M.Y. Saidi, R. Koksang, L. Morris, J. Power Sources 68 (1997) 291.
- [22] F. Cao, I.V. Barsukov, H.J. Bang, P. Zaleski, J. Prakash, J. Electrochem. Soc. 147 (2000) 3579.
- [23] J.R. Dahn, A.K. Sleight, H. Shi, J.N. Reimers, Q. Zhong, B.M. Way, Electrochim. Acta 38 (1993) 1179.
- [24] W. Qiu, G. Zhang, S. Lu, Q. Liu, Solid State Ionics 121 (1999) 73.
- [25] H. Shi, J. Baker, M.Y. Saidi, R. Koksang, J. Electrochem. Soc. 143 (1996) 3466.
- [26] L.J. Hardwick, H. Buqa, P. Novak, Solid State Ionics 177 (2006) 2801.

- [27] W. Kohs, H.J. Santner, F. Hofer, H. Schrottner, J. Doring, I. Barsukov, H. Baqa, J.H. Albaring, K.-C. Moller, J.O. Besenhard, M. Winter, *J. Power Sources* 119–121 (2003) 528.
- [28] M.E. Spahr, H. Buqa, A. Wursig, D. Goers, L. Hardwick, P. Novak, F. Krnmeich, J. Dentzer, C. Vix-Guterl, *J. Power Sources* 153 (2006) 300.
- [29] M. Winter, P. Novak, A. Monnier, *J. Electrochem. Soc.* 145 (1998) 428.
- [30] M.E. Spahr, H. Wilhelm, J. Palladino, N. Dupont-Davlovsky, D. Goers, F. Joho, P. Novak, *J. Power Sources* 119–121 (2003) 543.
- [31] R. Yazami, D. Grerard, *J. Power Sources* 43–44 (1993) 59.
- [32] K. Yamaguchi, J. Suzuki, M. Saito, K. Sekine, T. Takamura, *J. Power Sources* 97–98 (2001) 159.
- [33] A. Mabuvhi, K. Tokumitsu, H. Fujimoto, T. Kasuh, *J. Electrochem. Soc.* 142 (1995) 1041.
- [34] M. Yoshio, R.J. Brodd, A. Kozawa, *Lithium-Ion Batteries; Science and Technologies*, Springer, 2009, pp. 330–331 (Ch. 18).